Wood Sci Technol (2014) 48:1019–1032
DOI 10.1007/s00226-014-0658-8

ORIGINAL

Uniaxial compression of rotationally symmetric Norway spruce samples: surface deformation and size effect

Michaela Zauner · Peter Niemz

Received: 19 March 2014 / Published online: 18 July 2014

Abstract The influence of size on strength is well known for various materials and testing methods, but not enough data and knowledge of the effect on wood under compressive strength can be found. Therefore, the deformation and compressive strength of hyperboloid Norway spruce samples were tested for different dimensions. To determine the influence of size on the strength, three different approaches were used: "weakest link theory", "size effect law" and "multifractal scaling law". Of the three scaling theories, the "size effect law" and the "weakest link theory" predicted the effect well. Additionally, to determine the surface deformation of various samples, DIC3D was used on the largest sample geometry. The experiments show the existence of a possible size effect during compression, while digital image correlation illustrates the expected differences in deformation due to the shape and dependence of the strain distribution on the structure of wood. Additional experiments are proposed to further verify the observed effects and expand the knowledge of the size effect.

Introduction

Between laboratory tests and practical application, differences in size and geometry of the specimens are usually found. This is especially true for laboratory tests involving additional measurement techniques and for wood with a limitation of the size of clear specimen due to the large differences in structure, as well as the inhomogeneity of the material. To enable a prediction of the properties of structures found in practical applications, knowledge of the differences in strength due to the

M. Zauner (✉) · P. Niemz
Department of Civil, Environmental and Geomatic Engineering, Institute for Building Materials, ETH Zurich, 8093 Zurich, Switzerland
e-mail: mzauner@ethz.ch

increasing size and changed geometry is needed. This applies to wood too, where the structural influences lead to differences between the theoretical and the real strain distribution.

The effect that strength decreases with increasing size has been investigated by several researchers. Best known in wood science is the so-called weakest link theory (WLT), formulated and experimentally verified by Weibull (1939a, b, 1951). It is a statistical theory, which is based on the idea that in a larger volume, the probability to encounter an element with lower strength is higher than in smaller volumes. In the end, this weakest element leads to the collapse of the structure. Weibull based the theory on perfectly brittle materials that fail at the initiation of macro-cracking (Bazant and Yavari 2005, 2007). The WLT was reformulated to equations with a power law, among others by Leicester (1973). Leicester introduced Eq. (1), with a characteristic size D, and A and s as constants;

$$\sigma_{\mathrm{N}} = AD^{-s} \tag{1}$$

Another approach was made by, e.g., Bazant (2000). For a small ratio of the characteristic size D to the radius of the fracture-process zone, he also formulated the WLT as a "power law" with the nominal strength dependent on the dimension of the characteristic size n_{d} and the Weibull parameter m:

$$\sigma_{\mathrm{N}} \alpha D^{-n_{\mathrm{d}}/m} \tag{2}$$

Additional theories are found in literature, mainly developed for quasi-brittle materials (mainly concrete). Two are frequently used and discussed: the "size effect law" (SEL; Bazant 1984) and the "multifractal scaling law" (MFSL; Carpinteri et al. 1994). SEL is based on linear elastic fracture mechanics and the strength theory, leading to the formula with the empirical constants B and D_0:

$$\sigma_{\mathrm{N}} = \frac{B}{\sqrt{1 + \frac{D}{D_0}}} \tag{3}$$

Finally, the MFSL is a phenomenological approach based on self-affinity of the structure and geometrical multifractality, with the empirical constants A and B:

$$\sigma_{\mathrm{N}} = \sqrt{A + {}^{B}/_{D}} \tag{4}$$

Both SEL and MFSL were developed for notched specimens where the stress tip is equally scaled with the specimen. The SEL was successfully applied to describe the size effect in fibrous material (PEEK), showing that the kink band found in fiber materials can be equaled to the crack (Bazant et al. 1999). Although both theories were developed for notched geometries, the stress concentration of samples with a cross-sectional area decreasing to a smallest area can be approximated to a notch (van Vliet and van Mier 2000; Van Mier and Van Vliet 2003).

Both the WLT and SEL were applied to wood in tension and bending. A size effect for tension perpendicular to the grain (Aicher 2010) and shear (Gappoev 1995; Morel and Valentin 1996) was successfully proven for SEL. The WLT has

been extensively used in wood testing. This includes bending (Madsen and Buchanan 1986; Madsen 1990; Piter 2012) and tension perpendicular to the grain (Barrett 1974; Pedersen et al. 2003).

To the knowledge of the author, only a few selected works exist for the WLT for wood under compression (e.g., Madsen 1992; Fotsing and Foudjet 1995), showing either no size effect (Fotsing and Foudjet 1995) or a small effect (Madsen 1992).

In addition to the size, the geometry and especially the distribution of structural elements (e.g., growth rings) influence the strain distribution and strength of a sample.

To evaluate the strains on the surface of specimen without extensive preparation, digital image correlation (DIC) is a viable method. DIC correlates movement of a random pattern (surface structure or applied pattern) caused by the deformation of the sample and with this determines the strains and stresses. Early works without (Choi et al. 1991) or with artificial speckle patterns (Zink et al. 1995) showed the applicability. The method is commonly used to, e.g., investigate variations in strain due to structure (Jeong et al. 2009; Lanvermann et al. 2014), influence of loading rate (Jeong et al. 2010), determination of bending (Haldar et al. 2011) and elasticity (Jernkvist and Thuvander 2001). To measure three-dimensional deformations and the deformation of curved surfaces, two cameras have to be synchronized. This has already been successfully used to evaluate deformations of wood (Ben Mbarek et al. 2011; Xavier et al. 2012).

Usually, simple geometries with rectangular shapes are used in testing, but in experiments conducted in synchrotron-based microscopic tomography, the low availability and small field of view necessitate methods to ensure a failure in a small predetermined region. This can either be realized through necking or notching. A notch leads to a cutting of cells in the actual failure region and if executed one-sided poses the threat of inducing one-sided stress concentrations and possible bending effects. Additionally, the stress distribution changes rapidly around the notch. Contrary to that, necking cuts cells above the smallest cross-section and leads to a slower change of stresses in the sample until reaching the highest stress concentration in the center. An example for necking in standardized testing is found in samples used to determine the tensile strength perpendicular to the fiber in a standard of the American Society for Testing and Materials (ASTM D 143).

To easily produce small samples for a synchrotron beamline with milling and to fill the field of view, a rotationally symmetric shape is desirable. The higher concentration of failure in the center of a rotationally symmetric shape and the subsequently higher failure rate in this region was shown in Zauner et al. (2012).

But due to the small size, the relationship between strength of those small samples and large structures cannot be fully determined without knowledge of the possible impact of the size effect.

Therefore, the strain distribution and size effect in a rotationally symmetric sample shape under compression, used in Zauner et al. (2012), were investigated in this paper. To the knowledge of the author, this combination has not been applied to wood before. First, the setup and data processing methods for the geometry are outlined. The experimental results show the influence of the structure, especially of the growth rings, on the strain distribution but additionally the expected strain

concentration due to the geometry. Despite the large influence of density, a size effect was visible in the samples. Further investigations are proposed at the end of the article.

Materials and methods

The rotationally symmetric specimens were designed to introduce a stress concentration in the center of the sample without notching. This was done to increase the probability of failure in experiments with limited availability. Although the principle sample shape may be used as a flat construct, a rotationally symmetric design was chosen because milling enables easy production of smaller sample shapes. A disadvantage of the shape is the difference in stress along the height of the sample that makes the measurement of the MOE difficult to accomplish. For an approximation, the deformation of the sample in a narrow region in the center may be used.

To verify or negate a possible size effect and to preserve the proportions, all dimensions were equally increased. All following shapes were derived from the sample shape used in Zauner et al. (2012). For geometry A in Fig. 1, all sizes were doubled: the radius increased to 6 mm, the smallest diameter to 2.6 mm and the height to 16 mm. For B, all dimensions were increased by 2.5, leading to a smallest diameter of 6.6 mm and a height of 40 mm. This was then doubled to get a smallest diameter of 13.2 mm and height of 80 mm for C. The last geometry was produced to allow an observation with DIC, increasing all dimensions of C by 1.2, with a smallest diameter of 15.8 (D).

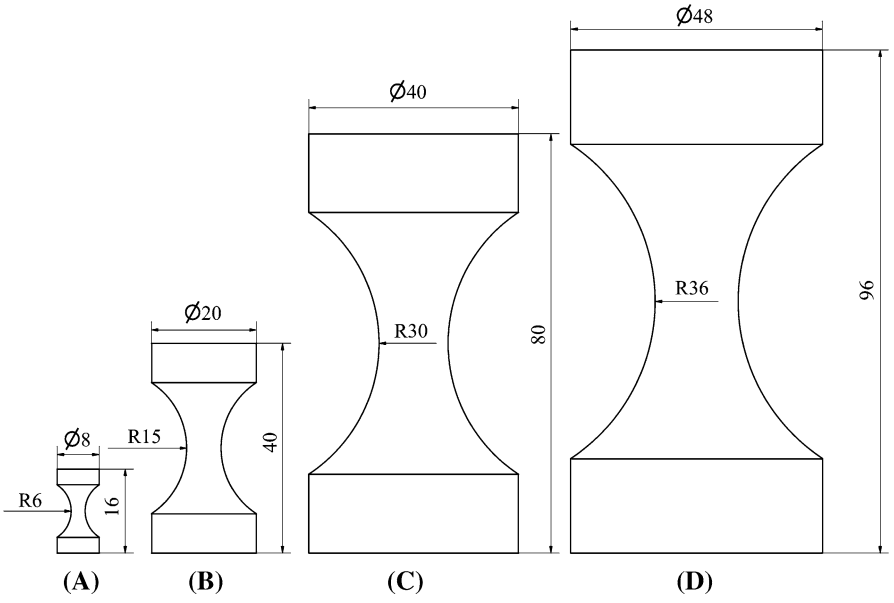

Fig. 1 Curved samples with enlarged dimensions, all values in mm

Table 1 Volume of the geometries in Fig. 1

Geometry	A	B	C	D
Volume (m^3)	4.6×10^{-7}	7.2×10^{-6}	5.7×10^{-5}	9.9×10^{-5}

The resulting volumes of all samples are listed in Table 1. As can be seen, the volume increases by one magnitude for every step between geometry A–C.

All samples were made of boards of adult Norway spruce wood (*Picea abies* [L.] Karst). The sample shape was realized in an automated CNC-milling machine, producing specimens with high accuracy and a smooth surface. Because of the long production time of up to 2 h, only a limited amount of samples was available.

In Fig. 2, the density of all samples is shown in boxplots. The highest variations in density were found for geometry C (475 ± 52 kg/m^3), where the growth ring width showed a high variation from 0.1 to 0.5 mm width with partly larger latewood zones of up to 0.2 mm. The density values of both geometries A (474 ± 36 kg/m^3) and B (429 ± 9 kg/m^3) were in the range of C but showed a more even year ring distribution of around 0.2 mm (0.1 up to 0.25). To allow a better observation of strains caused by structural differences, wood with broader growth rings (see Lanvermann et al. 2013) was chosen for the largest sample shape (D), leading to a decrease in density. Because of this, the samples showed significantly lower densities (352 ± 14 kg/m^3) with a year ring width of at least 0.5 up to 1.4 mm.

Reasons for the variation in density were the different percentages of softwood and latewood, which are not controllable during the processing due to the fact that a large part of wood is cut out in the center pieces. In combination with the cutout, the variation of the growth ring width in a wood board, difficulties in production and especially in controlling the exact position during the process, led to variations of density in the sample. The variation of the listed parameters as well as the more uneven direction of the growth rings in C led to the highest variations in density.

Method

All experiments were executed on a universal testing machine in norm climate (20° C, 65 %). The velocity of loading was determined to provide an equal increase

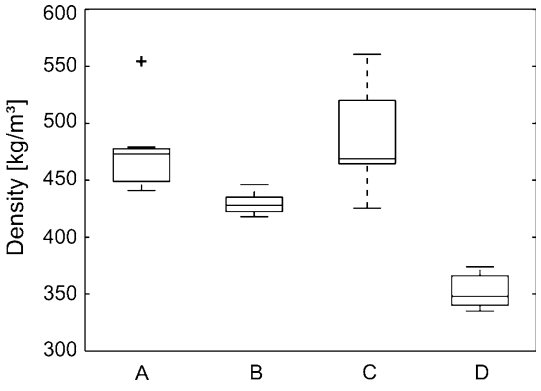

Fig. 2 Density of the four geometries in Fig. 1

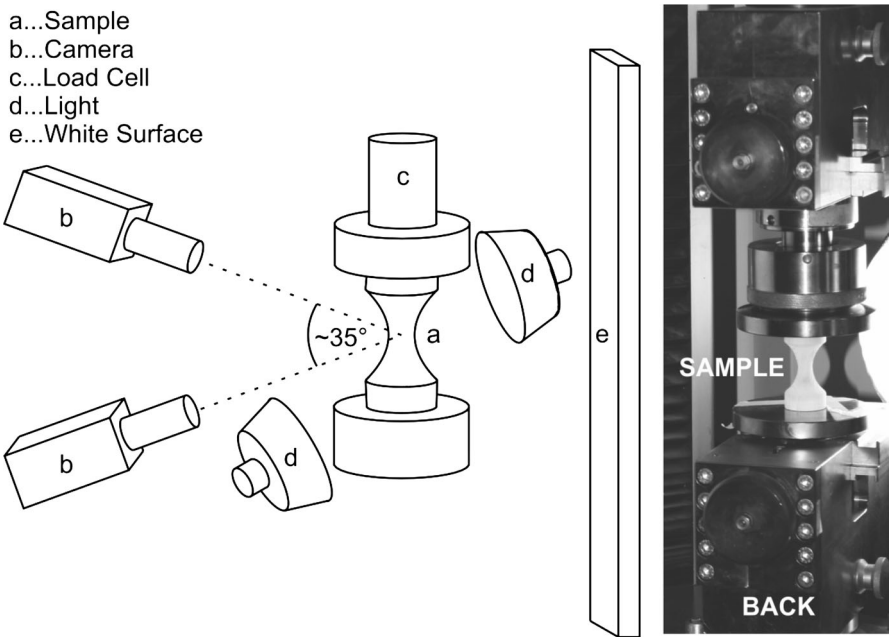

Fig. 3 Experimental setup to test different sizes of the curved sample shape

of strain/min of 0.0025 on all samples. To realize this, the velocities were increased with the same factor the dimensions were increased. Therefore, the velocities started with 0.04 mm/min for the smallest shape up to 0.1 mm/min, 0.2 mm/min and 0.24 mm/min for B–D, respectively.

To compare strains obtained directly through the testing device to other methods, the displacement of the crossbeam was recorded for all sample types. Additionally, the deformation of geometry D was monitored with 3D-DIC (Video Image Correlation (VIC 3D) version 2007, Correlated Solutions, USA). The setup is shown in Fig. 3. To enable a correlation, a black speckle pattern was applied with an airbrush pistol onto the white-coated surface of the sample. Two cameras were placed with an angle of 35° to each other to record images during loading. Due to the double-curved shape and despite the additional lightning and a white-reflecting surface placed around the sample, only a small portion of the sample surface could be sufficiently focused and recorded. The focal length used was 60 mm with an aperture of 3.5 mm and a shutter time of 29 min. Correlation of both images in space was done with a lattice of fixed points, recorded at different angles in place of the samples.

For the evaluation, a subset of 21 pixels with a step size of 5 was used and an average pixel size of 0.035 mm was the result. After the correlation, all subsequent processing steps were done in MATLAB.

Samples A and B were additionally monitored through extensometry. For this, two stripes with black and white horizontal bars were fixed on the upper and lower

end of each sample and recorded with a camera. The change of position of the stripes was then equaled to a deformation of the sample in this region.

To determine the strain with DIC, the calculated displacement of the elements in the FoV was averaged. Because of the low influence of errors on the borders, this was done for the complete selected area. All plots were boxed into equally spaced x-values to equalize them and negate outliers. Afterward, the plots were smoothed with an average moving filter with a span of 20 pixels. Stress values were determined in relation to the smallest diameter of the sample and with a preload of 10 N for geometry A, 60 N for B, 240 N for C and 350 N for D.

Results and discussion

The results of the mechanical testing of the above-mentioned samples are listed in Table 2. Due to the low resolution of geometry C, the values obtained with the DIC show a high deviation leading to inconsistent results and were therefore not used. The difference in density found in the samples is reflected in the compressive strength and the strain at compressive strength. Because of the higher deformability of a material with lower densities and lower stiffness and because of the known relationship between density and strength, this was to be expected.

Due to the curvature of the basic geometry, the strain values at compressive strength obtained over the complete sample deviate from the strain values obtained with extensometry or DIC (Table 2). Both geometries B and D have the lowest standard deviation of all samples, and the arithmetic mean strain value measured by extensometer or DIC is 30 % lower than for a measurement with traverse. The accumulation of the strain and the deviation during the complete stress–strain curve is shown for extensometry (B2) and VIC (D2) in Fig. 4. Two main differences are visible: In the curve measured over the complete sample length, a change of slope occurs at near 0.3 % strain for D and at the start of the curve for B. This behavior is more pronounced for the largest sample (D), probably due the differences in the geometry. Secondly and unexpectedly, the slope determined in a small section (after a starting section and up to 60 % F_{max}) is higher and leads to values similar to the MOE found in literature (e.g., 10,100 ± 1,500 for geometry D, 13,100 ± 1,200 for geometry B). A reason for the differences in behavior and the mechanical values is the large difference in density. For both of those geometries, the traverse–strain

Table 2 Compressive strength and strain determined with extensometry for geometry A and B and DIC3D for C and D, and traverse way, mean values (±SD)

Geometry	Density (kg/m^3)	Compressive strength (N/mm^2)	Ultimate strain (%)		Samples
			DIC/Ext.	Traverse	
A	474 ± 36	50 ± 5	0.65 ± 0.21	0.73 ± 0.12	8
B	430 ± 9	42 ± 1.5	0.43 ± 0.08	0.61 ± 0.03	11
C	486 ± 45	46 ± 7.5	0.62 ± 1.55	0.69 ± 0.14	12
D	352 ± 14	31 ± 2.5	0.37 ± 0.06	0.53 ± 0.02	9

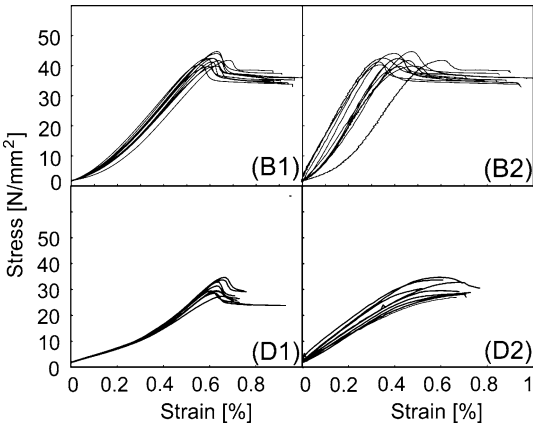

Fig. 4 Strain for samples B and D, measured by traverse leading to **B1** and **D1**, and with extensometry (**B2**) and VIC3D (**D2**), respectively

curves show a higher similarity to each other than measurements obtained in a limited area, probably because of the larger similarities over a complete sample. Changes mainly develop at the beginning of the curve. Overall and as expected, the traverse curves show deviations due to the specifications of the loading machine and differences in load introduction. Therefore, DIC, as well as extensometry, is preferable.

Two samples of geometry D were selected to observe the developing strains during increasing compression. The areas of the samples in the FoV of the camera are shown in Fig. 5. Here, the different orientation of the samples and the year rings are illustrated. While a view onto the tangential surface of the sample was monitored for Fig. 5a, the sample in Fig. 5b was slightly tilted for a mixed tangential–radial view. This leads to a distinct year ring structure on the left side of the sample, indicated by arrows. In Fig. 6, the respective stress–strain curves monitored by traverse (dot-line) and DIC are shown for the samples of Fig. 5. For those two samples, the compressive strength is 29 and 28 N/mm^2, while the density is 341 and 338 kg/m^3. While the traverse measured curves are nearly identical until reaching the compressive strength, the curves measured by DIC differ significantly. Figure 6b has a higher initial inclination that lowers to nearly identical values in the elastic region and decreases further to a lower inclination in the plastic region than for Fig. 6a. After reaching the compressive strength, both curves of Fig. 6b show a steeper declination.

Overall, the strain measured by traverse is nearly identical (0.52 against 0.51 %), and the measurement by DIC leads to values of 0.43–0.38 %.

The development of the strains is shown in Fig. 7. Initially, the strain on the sample is zero for both samples. As expected, the pattern that develops follows the year ring. This is especially evident in Fig. 7b. Overall, both samples show the same behavior: Major strains develop early on (starting before 50 % F_{max}) and further strengthen in a narrow band. Later on, additional strain fields can be observed (e.g., on the right side of Fig. 7b). The resulting failure line (visible in the last picture) is not predictable and develops late, although small excrescences are in the path of the failure line.

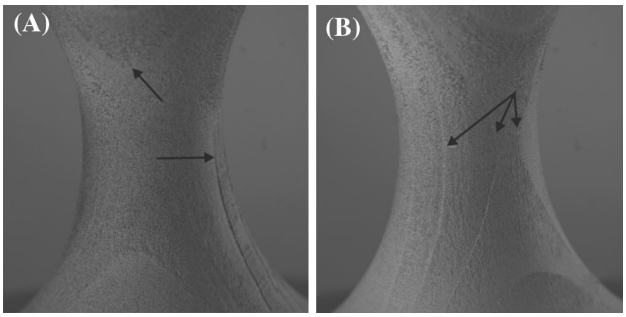

Fig. 5 Area in the field of view of the camera for two samples with *arrows* indicating visible growth *ring borders*

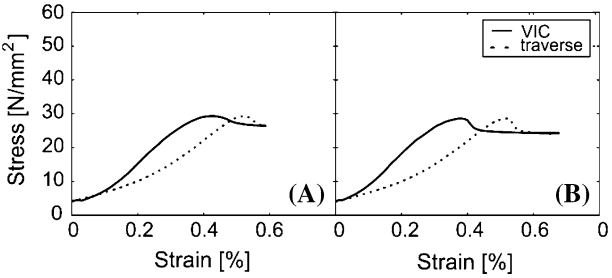

Fig. 6 Stress–strain curves monitored by 3D DIC and traverse (*dotted line*) for the two samples shown in Fig. 5

Similar to the approach above (Fig. 4), the mean value of the strain in the FoV leads to the usually observed overall strains. This can also potentially be done for different or smaller areas.

Size effect

The direct correlation of density and strength is well known. As expected, a correlation between strength and density was found for the samples used in the experiments. This is demonstrated in Fig. 8. Because of the large difference of density of geometry D in relation to the other geometries, as a first approach, the three size effect theories mentioned in the introduction [Eqs. (2)–(5)] were used on the three geometries A–C to obtain a fit and compare the fit for geometry D.

Following the convention to determine the size effect, the compressive strength is plotted against the diameter of the samples in a double logarithmic plot in Fig. 9. While Fig. 9a displays the original strength values, Fig. 9b shows normalized density values. The strength was normalized using the standardized raw density ρ_0 (1,500 kg/m^3) following the equation

$$\sigma_n = \frac{\sigma_i}{\rho_i}\rho_0 \text{ (e.g. Gindl and Teischinger 2002)} \quad (5)$$

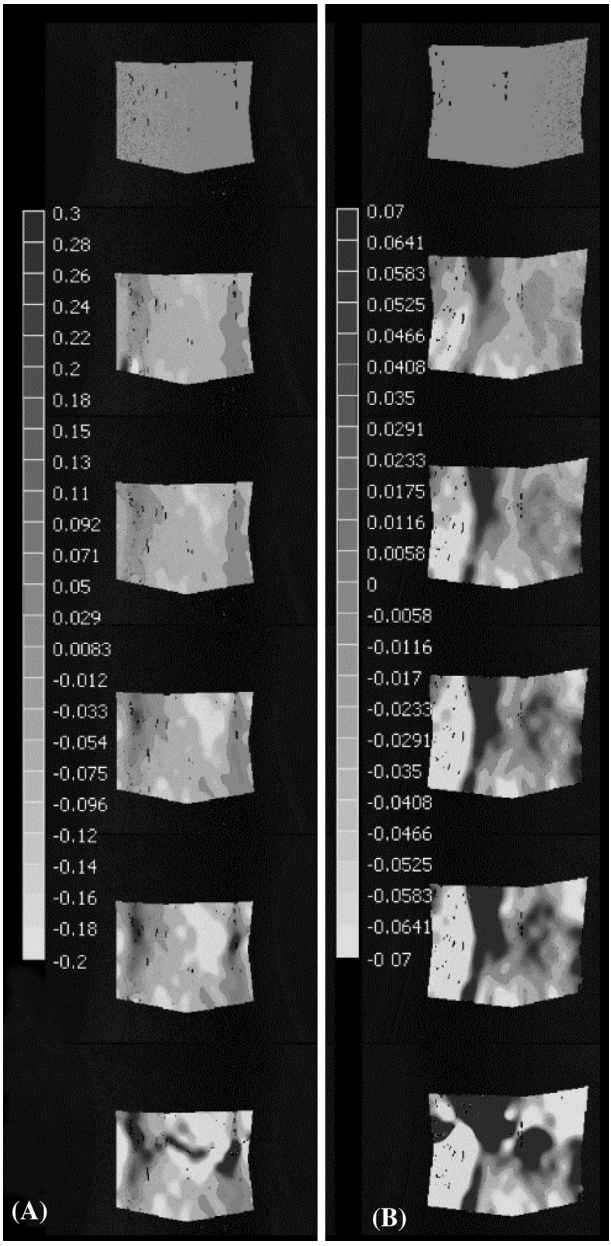

Fig. 7 Development of strain measured with a 3D DIC system, exemplary shown for two samples of geometry D; **a** sample in Fig. 5a and **b** sample shown in Fig. 5b—from *top* to *bottom*: at preload, 50 % F_{max}, 80 % F_{max}, F_{max}, F_{max} + 15 s, F_{max} + 30 s

The three size effect approaches were used for both versions shown in Fig. 9 for different reasons: SEL because of the larger size effect in theory, MFSL for comparison and the WLT because of the common use in wood testing. To determine

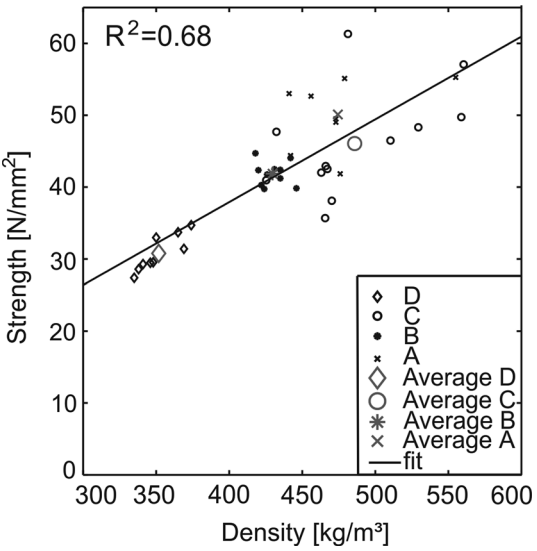

Fig. 8 Relationship between density and compressive strength sample sizes

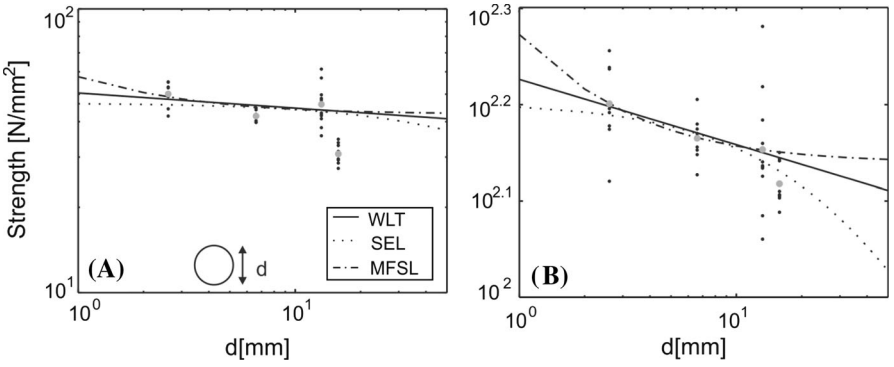

Fig. 9 Strength in relation to diameter tested for geometry A–C with power law (Weibull), SEL and MFSL with no correction (**a**) and with a density correction (**b**); *gray* mean values

the constants of the SEL, the inverse square root of the compressive strength was plotted against the proportional increase of the diameter. Afterwards, the empiric constants were obtained (after Bazant 1984; Aicher 2010) with the parameters of the fitted curve in a graph with $y = \left(\frac{1}{\sigma}\right)^2$ and $x = d/d_1$. The resulting polynomial fit of first order ($y = ax + c$) is used to determine $D_0 = c/a$ and $B = 1/\sqrt{c}$.

The values of the fits depicted in Fig. 9a (original values) and Fig. 9b are listed in Table 3. Additionally, $g = \frac{3}{m}$ [m found Eq. (3)] was determined to compare the results of this approximation to literature values.

In the graph with not normed strength values (Fig. 9a), a grouping of geometries A and C, as well as B and D, is encountered due to the density. In particular, geometries B and D largely deviate from the fits. Using the corrected strength values

Table 3 Resulting variables of fits for SEL, MFSL and power law for measured strength and strength normed to raw density, shown in Fig. 9

	Original values	Normed values
D_0 (SEL)	89.5	40
B (SEL)	46.5	160
B (MFSL)	1,809	16,130
A (MFSL)	1,515	18,995
M (WLT)	56.2	44
a (WLT)	50.5	168

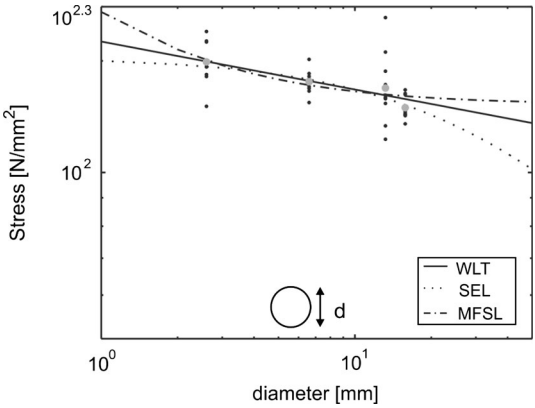

Fig. 10 Strength in relation to diameter equivalent to Fig. 9b but with geometries A–D tested power law (Weibull), SEL and MFSL with a correction of density; *gray* mean values

(Fig. 9b), the values are evened out and the average values for A–C can be found on the curves representing the three theories. Geometry D, which was not included in the calculation, is well included in the curve described by SEL, while MFSL leads to the highest deviations for values of geometry D.

Finally, Fig. 10 shows the result of the approximation of the size effect for all density-normed values of geometries A–D to compare it to the fit for geometries A–C found in Fig. 9b. Small differences to Fig. 9b are visible, but overall, both approaches lead to similar results—despite the large difference in density. This shows the good prediction of values found through WLT and SEL.

Conclusion

Overall, despite the more complex setup necessary, a hyperboloid shape in varying sizes is useable to test the behavior of wood and the traverse way can be used to monitor those samples, which was demonstrated when they were compared with other methods. A measurement with a DIC system leads to an observation of the expected deformation variations along year rings, while the average deformation equals the values expected from values measured over the length. With a higher resolution, the DIC system may be used to determine E-moduli of hyperboloid shapes. This could be done to extend the data obtained in measurements according to the ASTM standard (ASTM D 143) of tangential tension samples.

The difference in strength between samples in laboratory measurements at different dimensions and bigger constructions can be determined for geometries differing from common rectangular shapes. In the approximations of the size effect during compression, obtained by the three different theories: WLT (as power law), SEL and MFSL, the SEL and WLT lead to the most promising results. With a correction of the density, both theories allowed a prediction of the strength of samples with larger dimensions but lower densities. The damage mechanisms and therefore the strength of small samples used in Zauner et al. (2012) are comparable to the results found in the research in this work. Despite that, the comparability is lowered due to increasing probability of large EW- or LW-zones in small samples. This leads to a higher scatter of results and stronger outliers.

Due to limitations of sample production and the following relatively low amount of samples and dimensions, further studies to evaluate the applicable SELs are desirable. For an overall prediction for compression and tension, additional experiments with variable densities and geometries should be executed.

Acknowledgments I want to thank Klaus Rehm (Bern University of Applied Sciences, Biel) for producing the samples. This work was supported by the European Cooperation in the field of scientific and technical research (COST, Action FP0802).

References

Aicher S (2010) Process zone length and fracture energy of spruce wood in MODE-I from size effect. Wood Fiber Sci 42:237–247

Barrett JD (1974) Effect of size on tension perpendicular-to-grain strength of Douglas-fir. Wood Fiber Sci 6:126–143

Bazant ZP (1984) Size effect in blunt fracture: concrete, rock, metal. J Eng Mech-Asce. 110:518–535

Bazant ZP (2000) Size effect. Int J Solids Struct 37:69–80

Bazant ZP, Yavari A (2005) Is the cause of size effect on structural strength fractal or energetic-statistical? Eng Fract Mech 72:1–31

Bazant ZP, Yavari A (2007) Response to A. Carpinteri, B. Chiaia, P. Cornetti and S. Puzzi's comments on "Is the cause of size effect on structural strength fractal or energetic-statistical?". Eng Fract Mech 74:2897–2910

Bazant ZP, Kim JJH, Daniel IM, Becq-Giraudon E, Zi G (1999) Size effect on compression strength of fiber composites failing by kink band propagation. Int J Fract 95:103–141

Ben Mbarek T, Robert L, Hugot F, Orteu JJ (2011) Mechanical behavior of wood-plastic composites investigated by 3D digital image correlation. J Compos Mater 45:2751–2764

Carpinteri A, Chiaia B, Ferro G (1994) Multifractal scaling law for the nominal strength variation of concrete structures. In: Mihashi H, Okamura H, Bažant ZPE, FN SPON (eds) Size effect in concrete structures, pp 193–206

Choi D, Thorpe JL, Hanna RB (1991) Image-analysis to measure strain in wood and paper. Wood Sci Technol 25:251–262

Fotsing JAM, Foudjet A (1995) Size effect of 2 Cameroonian hardwoods in compression and bending parallel to the grain. Holzforschung 49:376–378

Gappoev MM (1995) Effect of specimen size on the crack resistance parameters in wood. Ind. Lab 61:101–104

Gindl W, Teischinger A (2002) Axial compression strength of Norway spruce related to structural variability and lignin content. Compos part a-Appl Sci Manuf 33:1623–1628

Haldar S, Gheewala N, Grande-Allen KJ, Sutton MA, Bruck HA (2011) Multi-scale mechanical characterization of Palmetto wood using digital image correlation to develop a template for biologically-inspired polymer composites. Exp Mech 51:575–589

Jeong GY, Zink-Sharp AE, Hindman DP (2009) Tensile properties of earlywood and latewood from loblolly pine (pinus taeda) using digital image correlation. Wood Fiber Sci 41:51–63

Jeong GY, Zink-Sharp A, Hindman DP (2010) Applying digital image correlation to wood strands: influence of loading rate and specimen thickness. Holzforschung 64:729–734

Jernkvist LO, Thuvander F (2001) Experimental determination of stiffness variation across growth rings in *Picea abies*. Holzforschung 55:309–317

Lanvermann C, Evans R, Schmitt U, Hering S, Niemz P (2013) Distribution of structure and lignin within growth rings of Norway spruce. Wood Sci Technol 47:1–15

Lanvermann C, Sanabria S, Mannes D, Niemz P (2014) Combination of neutron imaging (NI) and digital image correlation (DIC) to determine intra-ring moisture variation in Norway spruce. Holzforschung 68(1):113–122

Leicester RH (1973) Effect of size on the strength of structures. CSIRO Australian Forest Products Laboratory, Division of Building Research Technological Paper No. 71, 1–13

Madsen B (1990) Size effects in defect-free Douglas-fir. Can J Civil Eng 17:238–242

Madsen B (1992) Structural behaviour of timber. Timber Engineering LTD, Vancouver

Madsen B, Buchanan AH (1986) Size effects in timber explained by a modified weakest link theory. Can J Civil Eng 13:218–232

Morel S, Valentin G (1996) Size effect in crack shear strength of wood. J Phys IV 6:385–394

Pedersen MU, Clorius CO, Damkilde L, Hoffmeyer P (2003) A simple size effect model for tension perpendicular to the grain. Wood Sci Technol 37:125–140

Piter JC (2012) Size effect on bending strength in sawn timber of fast-growing Argentinean Eucalyptus grandis. Analysis according to the criterion of European standards. Eur. J. Wood Wood Prod. 70:17–24

Van Mier JGM, Van Vliet MRA (2003) Influence of microstructure of concrete on size/scale effects in tensile fracture. Eng Fract Mech 70:2281–2306

van Vliet MRA, van Mier JGM (2000) Experimental investigation of size effect in concrete and sandstone under uniaxial tension. Eng Fract Mech 65:165–188

Weibull W (1939a) The phenomenon of rupture in solids. Ingeniörs Vetenskaps Akademien-Handlingar. Generalstabens Litografiska Anstalts Förlag, Stockholm

Weibull WA (1939b) Statistical theory of the strength of materials. Ingeniörsvetenskapsakademiens Handlingar. Generalstabens Litografiska Anstalts Förlag, Stockholm

Weibull W (1951) A statistical distribution function of wide applicability. J Appl Mech-T Asme 18:293–297

Xavier J, de Jesus AMP, Morais JJL, Pinto JMT (2012) Stereovision measurements on evaluating the modulus of elasticity of wood by compression tests parallel to the grain. Constr Build Mater 26:207–215

Zauner M, Keunecke D, Mokso R, Stampanoni M, Niemz P (2012) Synchrotron-based tomographic microscopy (SbTM) of wood: development of a testing device and observation of plastic deformation of uniaxially compressed Norway spruce samples. Holzforschung 66:973–979

Zink AG, Davidson RW, Hanna RB (1995) Strain-measurement in wood using a digital image correlation technique. Wood Fiber Sci 27:346–359